CHAPTER 4.2

Temporally shaped femtosecond laser pulses for creation of functional sub-100 nm structures in dielectrics

Nadine Götte[1], Thomas Kusserow[3], Thomas Winkler[1], Cristian Sarpe[1], Lars Englert[2], Dirk Otto[1], Tamara Meinl[3], Yousuf Khan[3], Bastian Zielinski[1], Arne Senftleben[1], Matthias Wollenhaupt[2], Hartmut Hillmer[3], Thomas Baumert[1]

[1] University of Kassel, Institute of physics and CINSaT, Heinrich-Plett-Str. 40, D-34132 Kassel
[2] University of Oldenburg, Institute of physics, Carl-von-Ossietzky-Straße 9-11, D-26129 Oldenburg
[3] University of Kassel, Institute of Nanostructure Technologies and Analytics and CINSaT, Heinrich-Plett-Str. 40, D-34132 Kassel

Abstract

Material processing of dielectrics by temporally shaped femtosecond laser pulses will be presented in the following chapter. Structures with feature sizes in the sub-100 nm range are created and the motivation for their application in optical devices is given. The properties of our processing method are discussed with respect to the ionization effects of the light-matter interaction and the implemented tailored pulse shapes to address these individually. Experimental results of structures created in dielectric solids are shown. Electron densities in a water jet were studied numerically and by spectral interferometry to confirm a model for the light-matter interaction. The application and characterization of fabricated patterns with regard to the implementation of an optical filter element were studied by numerical simulations and experimental methods.

4.2.1 Application and processing of dielectric materials for optical devices

A large variety of optical elements are made from dielectric materials. For example lenses and prisms for free space optics as well as optical fibers and of course thin-film coatings or optical MEMS (Micro-Electro-Mechanical Systems) – they all are based on the distinctive properties of dielectrics [1]. The main advantage is their low absorption over a wide spectral range, which makes them in most cases applicable from the UV to the near-IR. Processing technologies to produce, deposit or structure these materials are well established and low-cost when compared to other optical materials, like III/V semiconductors. Optical properties and other important parameters can be varied by choosing the appropriate group of dielectric materials. Fluorides, like MgF_2 and CaF_2, are highly transparent far into the UV range and own very low refractive indices, but are often hygroscopic and show low mechanical stability. Nitrides, like Si_3N_4 or AlN, are more stable and have a higher refractive index around n = 2, but become absorbing for UV wavelengths. The most common group of dielectrics in optical applications are oxides, which can own low refractive indices around n = 1.5, like SiO_2, or are located in a medium range below n = 2, like Al_2O_3, but reach also up to higher indices, like ZrO_2, Nb_2O_5 or TiO_2. Oxides are in general mechanically and chemically quite stable and can hence be applied if long-term durability is required. For our investigation on processing of dielectrics by temporally shaped fs-laser pulses we focused only on amorphous or poly-crystalline oxides as these feature most beneficial properties.

The optical properties of a dielectric material are mainly defined by the band gap energy, which is ranging at least between E_{gap} = 5 eV … 10 eV, and a Fermi level well below the lowest energy of the conduction band. Due to the high band gap energies, light in the near-IR, visible or even UV range is not absorbed, as the energy of single photons is not sufficient. Since the conduction band is not occupied by electrons the materials are also electrically insulating, which actually defines the term „dielectric" [2].

Optical elements with Nanostructures

The interaction of waves with a structure shows the strongest effects if the feature size of the structure is of the same order as the wavelength or below. For the optical spectral range between λ = 200 nm … 2000 nm, structures with sub-µm dimensions or nanostructures are hence required. Feature sizes between approx. $\lambda/4$ and a few λ lead to superposition of waves. This effect can be enhanced if a periodic pattern of the structure is implemented, resulting in constructive, destructive or resonant behavior, respectively. Patterns with 1D periodicity are for example diffraction gratings or multi-stacks of thin-films. By extending the periodic properties to 2D or 3D, photonic crystals are obtained which can be described in analogy to the behavior of electrons in a crystalline structure [3]. Photonic crystal devices are commonly fabricated in semiconductor materials, which have excellent properties but limit their use to the near-IR. Similar structures in dielectrics have been reported [4] with promising results and will be the subject of the first test of our material processing method using fs-laser pulses.

When nanostructures with feature sizes far below the target wavelength are considered, rather different interaction effects will take place. First, scattering of light can be observed and tailored by appropriate structures [1]. A second approach is the generation of artificial refractive index materials by using the spatial averaging properties of the incident wave [5]. Finally, the near field of optical waves can be accessed, analyzed and manipulated, leading to an entirely new type of optics [6]. These effects are mainly observable for feature sizes between $\lambda/100$ and $\lambda/10$, shifting structures even for applications in the near-IR range to the sub-100 nm range. Thus, creating such structures by temporally shaped fs-laser pulses will be a promising method for future applications.

**Fabrication of Nanostructures in dielectric materials**

Creation of nanostructures in dielectric materials can be rather challenging due to various reasons. The most conventional methods are based on serial lithography by exposure of a resist material (e.g. PMMA) to an electron beam or direct ion milling of the dielectric with the help of a focused Ga^+ ion beam. Both methods are well established, commercially available and can reach down to feature sizes as small as a few tens of nanometers [7] [8]. In the case of electron beam lithography further processing steps to transfer the pattern to the dielectric material are required. The main disadvantage of these methods, when dielectrics are considered, is the accumulation of charges at the sample surface. As the beams interact with the material, charged particles of the beam and secondary charged particles due to inelastic scattering appear. For a conducting sample they discharge via the sample stage which is electrically grounded. As dielectric materials are by definition insulating, no charge transfer can take place and surface charging occurs which deteriorates the incident focus beam and makes high quality patterning unfeasible. A common workaround when structuring dielectric materials is to coat the surface with a thin conductive layer, for example sputtering or evaporating Pt or Au with a thickness of 10 nm. Aside from the additional processing steps of deposition and removal, the surface roughness of these thin metal films is likely to reduce the achievable pattern quality if feature sizes in the sub-100 nm range are desired. Another option is to implement active charge compensation by either installing a source of inversely charged particles that are exposed to the sample surface during lithography or by increasing the pressure in the vacuum chamber and exploit charge transport and compensation by residual gas molecules. Both methods require additional complex components in the lithography system and add other undesired effects. Furthermore, the discussed lithography processes require high vacuum conditions to provide sufficient free mean path lengths for the particle beams. This can render problematic if samples with pores or closed cavities are considered as well as for samples which contain outgassing materials.

Optical lithography can overcome the problems of charging and does not depend on vacuum conditions. Serial laser beam exposure of a photoresist, however, cannot reach to resolutions in the sub-100 nm range due to the diffraction limit. Making use of stimulated emission depletion however has the potential to overcome this

barrier [9]. In commercial photo-lithography, mask projection is employed for mass production and feature sizes of a few ten nanometers are the state of the art [10]. The use of deep UV, vacuum UV or even extreme UV light and the extremely high complexity of the related processing make this approach though economically not justifiable for smaller batches or research. In recent years nanoimprint technology has become more and more competitive for reproduction of nanostructures and may be a good option for the discussed applications. But as a master template for the imprint has to be fabricated, still the demand for a primary structuring method exists.

Our approach to use temporally shaped fs-laser pulses (λ = 800 nm) for sub-100 nm material processing combines the advantages of optical lithography with direct structuring techniques and the resolution of focused charged particle beams. Since photons are used no charging effects occur and no vacuum conditions are required. By employing nonlinear optical ionization effects and addressing them individually by tailored pulse shapes, material ablation far below the diffraction limit has been achieved [11]. Complex patterns of nanostructures are generated with the help of a piezo stage, scanning the sample in relation to the laser focus. Lateral dimensions as well as the depth of the structures can be controlled by adjusting the exposure dose.

Different experiments have shown that laser-induced damage thresholds are strongly dependent on the laser pulse duration [12] [13] [14] and its temporal shape [11], respectively. An exemplary pulse selection is shown in Sec. 4.2.3. This can be attributed to the influence of the pulse characteristics on the ionization processes and temporal evolution of free electron density [15] [16], as will be discussed in Sec. 4.2.2. Furthermore, it has been demonstrated that direct structuring of dielectric materials with temporally shaped femtosecond laser pulses [11] [17] [18] and double pulses generate reproducible structures with dimensions down to one order of magnitude below the diffraction limit (sub-100 nm structures, compare Fig. 1). Femtosecond pulse manipulation techniques play a major role in many applications [19] [20] [21].
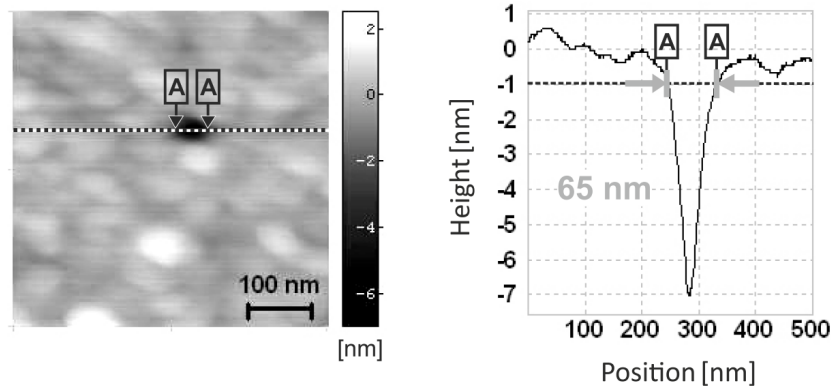

Fig. 1: Exemplary sub-100 nm hole in fused silica generated via a single double pulse with an inter-pulse delay of 3.0 ps and a total pulse energy of E=122 nJ. The surface diameter of d = 65 nm was measured via atomic force microscopy (resolution 1 pixel/nm) [57] (unpublished).

3

4.2.2 Laser material processing of dielectrics via short and ultrashort laser pulses

As mentioned before, most advantages of the conventional, primary structuring processes are combined in the alternative approach with fs-laser. For goal-oriented material processing comprehensive knowledge of the material, in this case the dielectric and its interaction with the laser is necessary. Hence the following section will give a short summary of the current state of research.

4.2.2.1 Fundamentals: Light-matter interaction of dielectrics and pulse shaping

Transparent dielectric materials, e.g. glasses, become highly absorbing by applying ultrashort laser pulses with sufficient intensities [22] [23]. As soon as the laser pulse exceeds a certain intensity it is able to generate small numbers of free electrons. In turn, this so produced plasma is highly absorbing for the later parts of the laser pulse [11] [24]. The first step is accomplished by multi-photon ionization[1] (MPI), which is related to the wide band gap of the dielectric in relation to the photon energy. It is well known, that the probability of MPI is proportional to I^n, where I is the intensity of the laser pulse and n the number of photons required to overcome the band gap. These first few electrons can be considered as seed-electrons for avalanche ionization (AI). AI is a two-step process, where an electron in the conduction band gains kinetic energy by free carrier absorption (inverse Bremsstrahlung) and impact ionizes another electron from the valance band (compare Fig. 2). Please note that in laser material processing the expressions "ionization" and "free electrons" are commonly equivalent to "excitation" and "conduction band electrons", respectively [23].
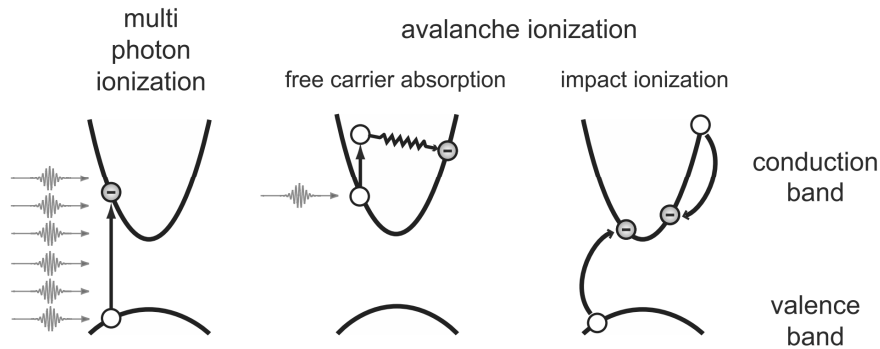

Fig. 2: Generation of a high density of free electrons in dielectrics. Left: Six photons are simultaneously absorbed by the electron from the highly intense laser pulse to overcome the band gap. Right: The combination of free carrier absorption and impact ionization is known as Avalanche ionization. An existing electron in the conduction band can absorb single photons to increase its energy. Since the electron has sufficient energy it can impact ionize a valence band electron.

The relevance of the different ionization channels is strongly related to the temporal shape of the ultrashort laser pulses, as will be discuss in detail later. But first we want to expand on the typically employed pulse shapes, by giving the basic mathematic description and examples. An overview of the four basic classes of pulse shapes we typically applied is represent in Fig. 3.

A more detailed representation – comprising pulse shaping technique via spectral phase modulation – can be found e.g. in Ref. [17] [25] [26].

---

[1] In general strong field ionization contains MPI and tunnel ionization. Due to the relatively low intensities in the experiments tunnel ionization only contributes in a minor fashion and can be neglected.
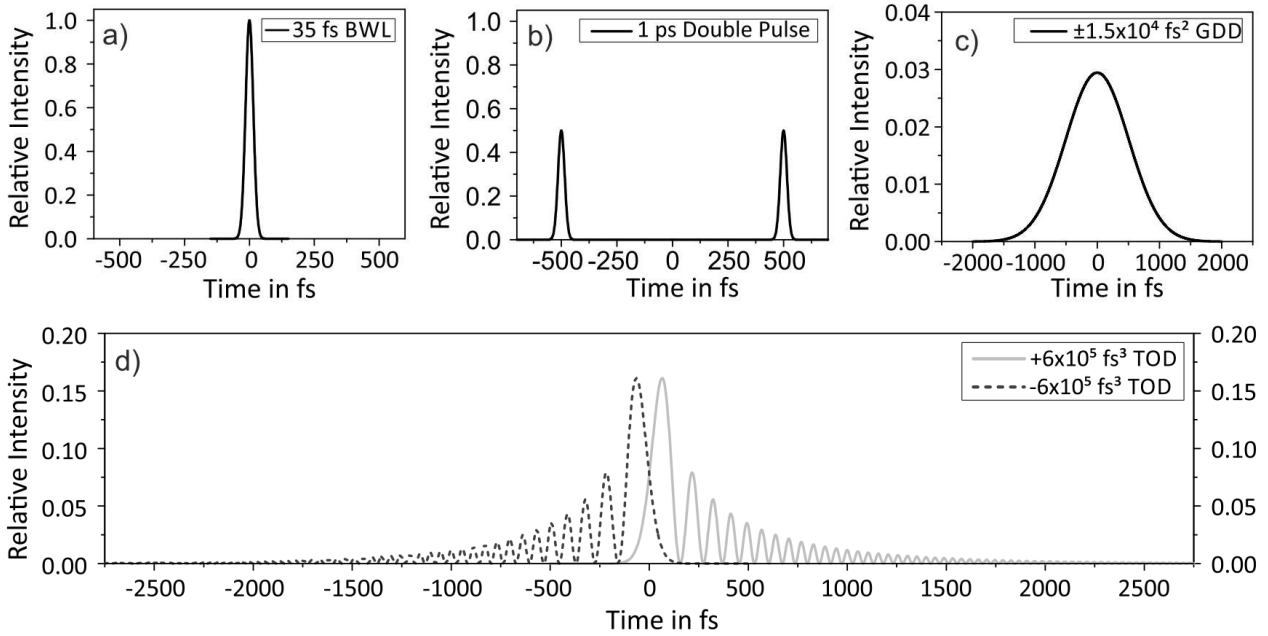
Fig. 3: All pulses are simulated with the same total pulse energy and are intensity normalized to the bandwidth-limited pulse (BWL) with a FWHM pulse duration of τ = 35 fs (a). BWL pulse with a FWHM pulse duration of τ = 35 fs (a), double pulses (each pulse τ = 35 fs) with an inter-pulse delay of $\Delta\tau = 1\text{ps}$ and an intensity ratio of 1:1 (b). BWL pulse subjected to a second order dispersion (GDD) of $\phi_2 = \pm 1.5 \cdot 10^4 \text{fs}^2$ (c) and BWL pulse subjected to a third order dispersion (TOD) of $\phi_3 = \pm 6 \cdot 10^5 \text{fs}^3$ (d) leading to a pulse duration of $\tau \approx 1\text{ps}$, respectively.

a) Bandwidth-limited ultrashort laser pulses

The first class of pulses are ultrashort bandwidth-limited pulses (BWL) with Gaussian temporal pulse envelope (Fig. 3a) and a full width at half maximum (FWHM) pulse duration of τ = 35 fs. Since MPI requires a highly intense laser pulse and requires no initial free electrons, it has the highest efficiency for the generation of a high free electron density for pulses shorter than approx. 50 fs. In contrast, due to the shortness of the pulse, there is no time for AI to establish and AI can therefore be neglected. The BWL pulse has the lowest energy threshold for material ablation and the according pulse envelope of such an unmodulated pulse can be mathematically described as

$$\mathcal{E}(t) = \frac{\mathcal{E}_0}{2} \cdot \exp\left[-\ln(4)\left(\frac{t}{\tau}\right)^2 \right]$$

With an amplitude $\mathcal{E}_0$ of the pulse and τ is the unmodulated pulse duration. The instantaneous frequency is constant throughout the unmodulated pulse and the spectral phases are constant (in contrast to parabolic and cubic phase for GDD and TOD, see below).

b) Chirped laser pulses by group delay dispersion (GDD)

The second class is represented by linearly chirped pulses with varying instantaneous frequency ω(t) (Fig. 3c). Their spectrum and the symmetric, Gaussian temporal pulse envelope are identical to those of BWL pulses, but in comparison the peak intensity is reduced due to temporal broadening of the pulse (energy conservation).

Group delay dispersion (GDD) is introduced by applying a parabolic spectral phase function $\varphi(\omega) = \frac{\phi_2}{2} \cdot \omega^2$ to

the spectrum $\tilde{\mathcal{E}}(\omega)$ ($\tilde{\mathcal{E}}_{mod}(\omega) = \tilde{\mathcal{E}}(\omega) \cdot e^{-i\varphi(\omega)}$) and ϕ_2 is the so-called chirp parameter. A positive value of ϕ_2 leads to an up-chirped pulse characterized by a linear increase of the instantaneous frequency in time, whereas a negative value of ϕ_2 implies a decrease of the instantaneous frequency, known as down-chirp. The modulated FWHM pulse duration for a chirped Gaussian pulse is

$$\tau_{GDD} = \sqrt{\tau^2 + 16 \cdot [\ln(2)]^2 \left(\frac{\phi_2}{\tau}\right)^2}$$

Therein τ denotes the unmodulated pulse duration and ϕ_2 the chirp parameter. The higher ϕ_2 the more pronounced is the temporal broadening. When the pulse duration exceeds 50 fs the avalanche ionization can no longer be neglected for free electron generation.

c) Temporally asymmetric shaped laser pulses by third order dispersion (TOD)

The third class of pulses is characterized by an elongated pulse duration and an asymmetric pulse envelope. The instantaneous frequency – and therefore the photon energy provided by the pulse – is constant over the course of the whole pulse. Third order dispersion (TOD) is introduced by applying a cubic spectral phase function $\varphi(\omega) = \frac{\phi_3}{6} \cdot \omega^3$ to the spectrum $\tilde{\mathcal{E}}(\omega)$ and ϕ_3 is the dispersion parameter of third order. This leads to a modulated pulse shape, which is characterized by an intense initial pulse followed by a sequence of pulses with decaying amplitudes. The sign of ϕ_3 controls the temporal direction of the pulse shape: positive values of ϕ_3 lead to a series of post-pulses whereas negative values of ϕ_3 result in a series of pre-pulses (Fig. 3d).

Since TOD pulses are asymmetrically broadened in time, the temporal FWHM is no longer a suitable property to describe the pulse duration. Therefore, we use the statistical pulse duration[2] $2\sigma = \tau / \sqrt{2\ln 2}$ [25] to describe the pulse duration. Since the statistical pulse duration 2σ delivers shorter values for an unmodulated Gaussian pulse compared to the FWHM, we define the modulated pulse duration by $\tau_{mod} = \sqrt{8 \cdot \ln(2)} \cdot \sigma$ to obtain a quantitative measure of the pulse duration

$$\tau_{TOD} = \sqrt{\tau^2 + 16 \cdot [\ln(2)]^3 \left(\frac{\phi_3}{\tau^2}\right)^2}$$

[26] that agrees with the FWHM of the unmodulated pulse.

### d) Bandwidth-limited double pulses with 1:1 ratio

The last class of laser pulse shapes that were applied in our studies for material processing are BWL, Gaussian shaped double pulses with varying inter-pulse delay and an intensity ratio 1:1 (Fig. 3b). The generation with a polarization pulse shaper of such pulse shapes is described in detail in [27].

---

[2] The statistical definition of the pulse duration derived with the help of the second moment of the intensity distribution uses twice the standard deviation σ to characterize the pulse duration.

4.2.3 Experimental results in dielectrics

4.2.3.1 Fused silica SiO2

The results obtained from our earlier experiments [11] [28] are summarized in Fig. 4. Systematic studies with phase shaped laser pulses based on TOD leading to asymmetric temporally shaped laser pulses revealed a change in the damage threshold depending on whether the direct (positive ϕ_3) pulse shape or the time inverted profile (negative ϕ_3) was used [see Fig. 4a]. Theoretical simulations based on a multiple rate equation (MRE) model described in Ref. [15] show that it is the timing of an intense photo-ionizing sub-pulse which can turn on AI or not. The observed nanoscale structures are an order of magnitude below the diffraction limit and remarkably stable with respect to variations in laser fluence [see Fig. 4c]. Applying pure second order dispersion at threshold, also sub-diffraction structures are created; however, no substructure being stable with respect to laser fluence variations was observed [26].
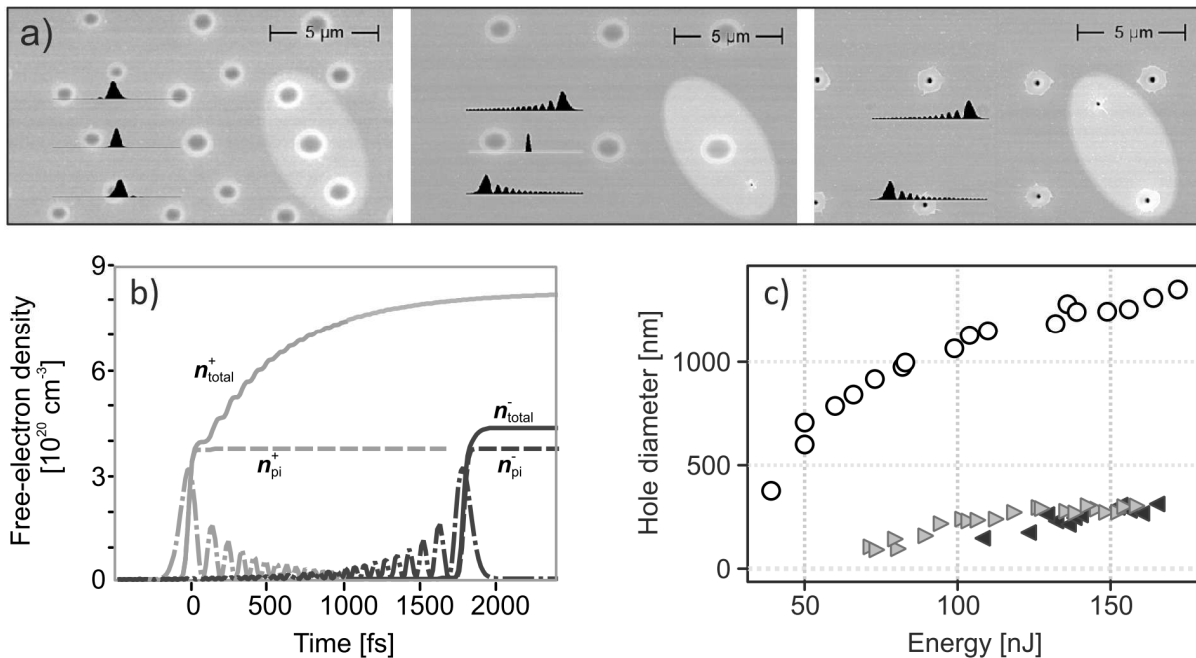
Fig. 4: (a) SEM micrographs of a measurement pattern on fused silica: For an applied energy E and focal position, a triplet of applied laser pulses is highlighted by the ellipse. Negative, zero, and positive TODs were used where the corresponding normalized temporal intensity profiles are sketched in black for different TODs. Left: low TOD ($\phi_3 = \pm2.5 \cdot 10^4\,\text{fs}^3$, statistic pulse duration of 2σ = 50 fs, E = 77 nJ) results in negligible differences between created structures. Middle: high positive TOD ($\phi_3 = +6 \cdot 10^5\,\text{fs}^3$, statistic pulse duration of 2σ = 960 fs, E = 71 nJ) results in a change of structure size and threshold energy. Right: the threshold energy for ablation with high negative TOD ($\phi_3 = -6 \cdot 10^5\,\text{fs}^3$) is reached with E = 110 nJ. Here, the unshaped pulse is suppressed in order not to mask structures with TOD. (b) Transient free electron density n_{total} (solid lines) as calculated with help of the MRE, together with the density of electrons provided by photoionization n_{PI} (dashed lines), and the corresponding transient intensities (dashed-dotted lines) of the pulse with positive TOD (index +) and negative TOD (index −), respectively. (c) Inner diameters (compare Fig. 5) of ablation structures as a function of pulse energy for unshaped pulses (circles). For (+) shaped pulses (triangles pointing right) and for (−) shaped pulses (triangles pointing left), the diameter of the substructure is displayed. Without changing the focus spot diameter, substructures below 300 nm are obtained over a large energy range, thus providing a large process window for creation of nanostructures. The smallest structures are about 100 nm in diameter.

In Fig. 5, the observed morphologies for BWL pulses and TOD shaped pulses are summarized. Our original data were analyzed mainly via SEM (Scanning Electron Microscopy) and AFM (Atomic Force Microscopy). Recently, we turned to FIB characterization (Focused Ion Beam) in combination with SEM in addition. The maximum depth of the generated structures may be limited by the shape of the used high aspect ratio tip. The shape of the high aspect ratio tip is also responsible for the asymmetry in profile seen in Fig. 5b. At threshold, the structures are a few 10 nm in depth.
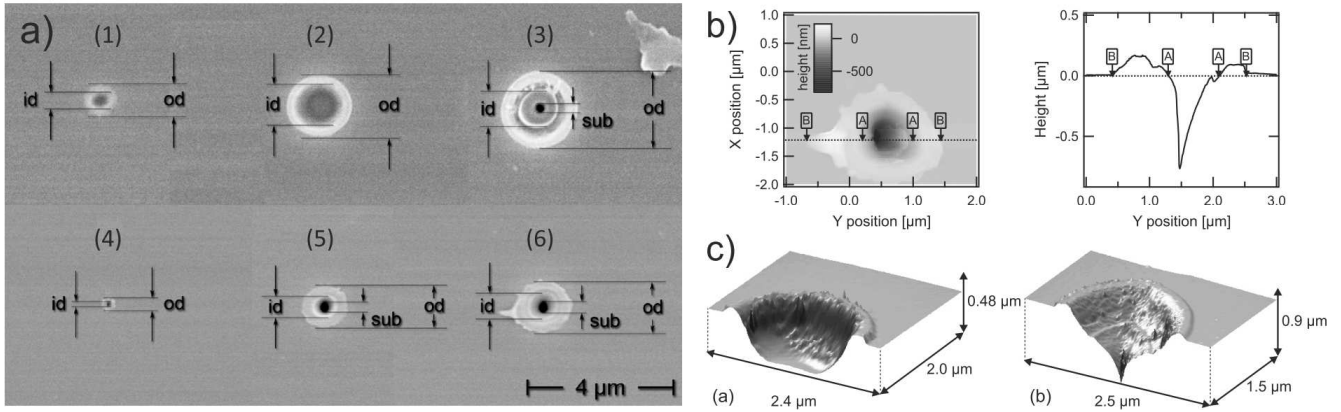
Fig. 5: (a) SEM micrographs for selected structures of Fig. 4c. *od* = outer diameter, *id* = inner diameter, and *sub* = diameter of substructure. For unshaped pulses at threshold for material processing (40 nJ) (1), at intermediate energy (140 nJ) (2), and at high energy (240 nJ) (3). Structures for high positive TOD ($\phi_3 = +6 \cdot 10^5 \, \text{fs}^3$) at threshold (4), at intermediate energy (120 nJ) (5), and at high energy (150 nJ) (6). At threshold, the substructure merges into the inner structure. For unshaped pulses, the substructure occurs only for high intensities and is embedded in a large area defined by the inner structure. (b) AFM image of structure a6. The distance BB defines the outer diameter *od* and AA defines the inner diameter *id*. Note the high aspect ratio of the 800 nm deep structure. As a general trend, the depth of the structures increased approximately linearly from the threshold up to 50 nJ above threshold in a range from several 10 to several 100 nm for positive and negative phase masks. (c) Typical AFM structures for the unshaped laser pulse. In the energy range up to 140 nJ, a shallow crater is observed (1), whereas in the energy range from 150 to 250 nJ, the additional small substructure appears (2).

The intriguing observation in Fig. 5 is that the observed substructure for unshaped pulses occurs only for high intensities and is embedded in a large area defined by the inner structure, whereas for the TOD shaped pulses, this substructure starts to appear already at threshold. On a first glance, the substructure might be attributed to filamentation processes as observed in bulk fused silica under similar excitation conditions [29] as well as on surfaces of dielectrics [30] [31] and reviewed in Ref. [32]. However, as filamentation usually needs propagation to occur, the lack of observed propagation structures especially for the TOD shaped pulses may rule out filamentation as the only explanation. Note that no plasma in air was observed at the applied laser energies, i.e. the used pulse energies for TOD are well below (factor of approx. 10) the critical power for self-focusing and filamentation processes. In order to investigate to what extent the seed and heat model explaining the differences in observed ablation threshold for temporally asymmetric pulse shapes may be extended to explain the spatial observations, we started simulations. The motivation stems from the simple picture that an initial part of the temporal pulse structure may create a free electron density well below the damage threshold via MPI in a spatially very confined region and the remaining pulse initializes AI to reach the critical energy also in a very restricted area. In those simulations, we solve rate equations for a Gaussian spatial beam profile taking MPI, AI and trapping into account as a function of various temporal profiles. So far we did not get a conclusive picture from these simulations: in the calculations, the threshold of material ablation was set by reaching a

certain electron density. This criterion allowed to describe the threshold for material ablation correctly for various temporal profiles, however, the structure diameter (inner structure) as a function of fluence was sometimes overestimated and sometimes underestimated compared to the measured ones. The substructure behavior was never reproduced in this approach. Currently we extend this approach to take propagation effects into account. Dedicated double pulse experiments up to 10 ps with the help of our latest pulse shaping setup [27] are currently performed in our labs in order to study early stage material modifications (see Fig. 1). An extension of the experiments to materials with different orders of the MPI process seems to be a promising route for a better understanding as well.

4.2.3.2 Experimental realization for fused silica

In our experiments, we combine femtosecond pulse shaping techniques [19] (that can reach nowadays zeptosecond precision) [27] with a microscope setup for material processing [11] [33]. Linearly polarized laser pulses with 35 fs FWHM pulse duration and a central wavelength of 790 nm are provided by an amplified Ti:Sapphire laser system. After passing a calibrated home built spectral phase modulator [34], the pulses are focused via a Zeiss LD Epiplan 50x/0.5 NA objective to a spot diameter of 1.4 μm ($1/e^2$ value of intensity profile). The dispersion of the objective was constantly compensated prior to the experiments. The pulse shaper is properly operated in a parameter regime far away from space time coupling effects [35] as verified also via quantum optical measurements with the same setup [36] [37]. Shaped pulses are characterized in the interaction region via second order cross correlation. The sample is translated by a 3-axis piezo stage to a new position for each shot (a single laser pulse). A typical measurement pattern consists of an array of points where we vary the pulse shapes, energy and focal z-position. After laser processing, the samples are analyzed via SEM and AFM.

4.2.3.3 Spectral interferometry: motivation and setup

Usually the influence of the temporal duration of laser pulses on the laser material processing is investigated via different post mortem techniques, such as AFM/SEM or optical microscopy. But this has the disadvantage, that between the excitation of the electrons and the final material ablation a large number of processes take place, which can't be directly observed this way. That is why we chose an in-situ measurement approach to directly observe the excitation of water in real-time with femtosecond resolution from the initial excitation up to 6.5 ps later. Water can be treated as an amorphous semiconductor with a reported energy band gap ranging from 6.5 eV [38] up to 8.3 eV and 12.4 eV [39] and shares the main ionization processes like solid dielectrics.

In our experiments, the laser pulses interact with a free flowing water jet, which ensures a new and fresh area of the sample for each laser pulse at repetition rate of 1 kHz.

Due to the fact that the optical breakdown process[3] is a general one, our findings can be well expanded to the behavior of solid dielectrics. In either cases the first step in the ablation process is the optical breakdown in which a high density of free electrons (around $10^{20} - 10^{22}\,\mathrm{cm}^{-3}$) is generated by the above mentioned nonlinear ionization processes. The free electrons absorb energy from the laser pulse, transfer it to the ions, atoms and molecules and, on a significantly longer time scale (several ps to ns), ablation can take place. The final features

---

[3] Optical breakdown describes the case when a transparent dielectric gets highly absorbing due to a high free electron density.

of the ablation process are strongly dependent on the primary processes involved in the laser-matter interaction.

We set up a common-path spectral interferometer to investigate in real-time the free electron density of the transient plasma produced by temporally asymmetric shaped ultrashort laser pulses in a thin water jet [24]. Spectral [40] [41] [42] [43] and spatial [44] [45] interferometry techniques are well established methods [46] to investigate the early time dynamics of laser excited dielectrics. In spectral interferometry a pair of probe and reference pulse, usually created in a Michelson line interferometer, is sent to an imaging spectrometer and frequency domain interference is produced. From the spectral interference data the phase shift – a reduction of the temporal separation of the probe pulse pair – and the transmission coefficient of the probe pulse can, for example, be obtained by inverse Fourier transformation [40]. Both quantities are directly dependent on the real and imaginary part of the complex refractive index of the excited sample, as seen by the probe pulse.

Inspired by [47], we make use of a common-path interferometer in which a pair of frequency doubled 400 nm reference and probe pulses ($\tau_{\mathrm{SHG}} = 50\mathrm{fs}$) are generated as ordinary and extraordinary beams when the light propagates through a birefringent crystal (see Fig. 6). The time delay between the pulses is defined by the thickness of the crystal. A second, thinner birefringent crystal, oriented 90 degrees with respect to the first one, is used to decrease the delay between the interfering pulses just before entering an analyzing spectrometer. This common-path approach leads to a stability much higher than in conventional interferometers.
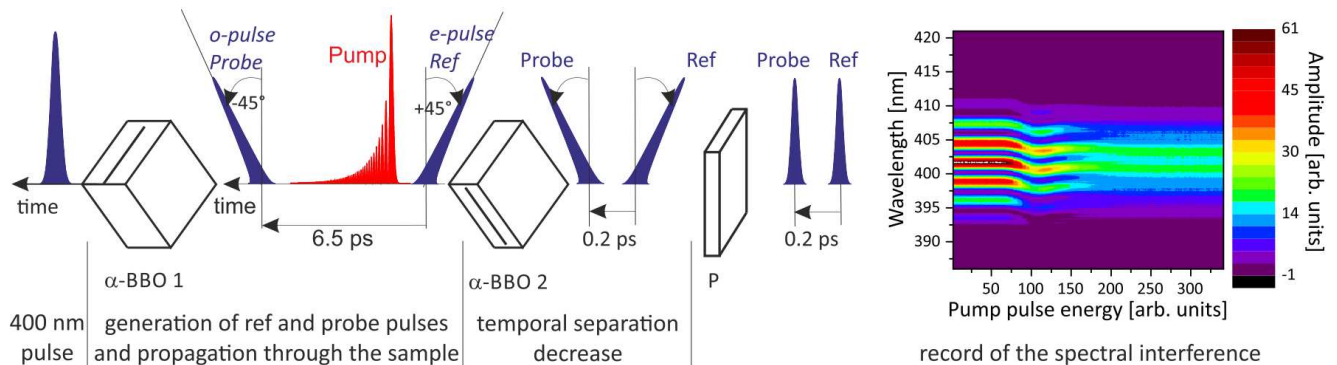
Fig. 6: From left to right: A time delayed pulse is frequency-doubled to 400 nm (blue pulses) and passes through a birefringent crystal α-BBO 1. This one creates a pair of orthogonally polarized pulses with a temporal separation of 6.5 ps. The reference and probe pulses propagate through the interaction area, together with the pump pulse (red pulse) in between, probing the changes in the optical properties. A second birefringent crystal α-BBO 2 decreases the temporal separation between the blue pulses to 0.2 ps. After passing through a polarizer (P) the frequency-domain interference pattern is recorded in a spectrometer, containing the optical properties of the excited sample. An example (raw-data) for a pump pulse energy dependent scan is shown.

A 800 nm shaped pump pulse is adjusted in such a way, that it creates the free carriers within the thin water jet inside the 6.5 ps time window between the reference and probe pulse (Fig. 6). The resulting phase difference and contrast of the interference fringes contains direct information about the optical properties of the plasma. This common path setup for the probe pulses was hitherto not used in combination with spectral interference. We demonstrated that it is a powerful tool to investigate the early and medium time dynamics of ultrafast processes [24].

### 4.2.3.4 Spectral interferometry: results on water jet

Our experimental realization of the spectral interferometry gives access to two main parameters of the resulting spectra: The phase shift $\Delta\Phi$ contains information about the real part of the refractive index of the water jet and the optical density *OD* about the free electron plasma absorption. From the combined data, the electron density and electron collision time τ_c can be evaluated by the well-known Drude formalism [48]. But, this is only directly possible as long as the sample is excited homogenously along the propagation direction of the laser pulse [45] [49], which can be assumed for low pump pulse intensities, compare Fig. 8B. Within this range the phase shift is directly proportional to the electron density.

In the following, the results of two investigations will be presented. The first section deals with the dependence of $\Delta\Phi$ and *OD* on the peak intensity of a BWL pump pulse. Subsequently the effect of positive and negative temporal asymmetrically shaped TOD pulses is investigated.

Please note that here we only present the pump pulse energy dependent excitation of water right after the BWL or TOD pump pulse has passed through the water jet. Time sensitive measurements over the whole 6.5 ps time window have been performed as well and are extensively discussed in [24].

Bandwidth-limited femtosecond pulses

Fig. 7 presents the dependence of the absolute phase shift and of the optical density on the peak pump laser intensity. For low intensities the dependence follows a power law indicated by the solid lines in Fig. 7, with an exponent of 5.1 ± 0.2 for the phase shift and 5.2 ± 0.2 for the optical density. This hints at a five-photon ionization process in the range of 0.1–0.8 rad as also expected from the band gap of 6.5 eV mentioned in the introduction section. With increasing pump intensity, the absolute phase shift also increases, but the assumption of a longitudinal homogeneous distribution is not valid anymore and the deviation from the straight line is evident.
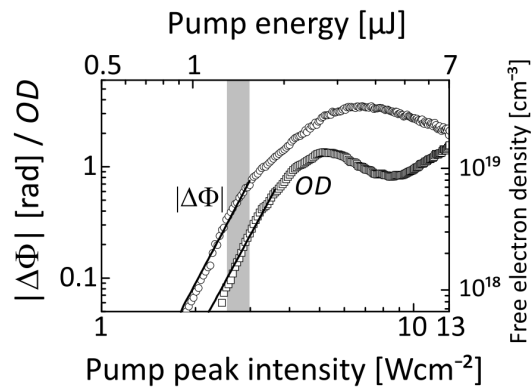
Fig. 7: Measured absolute phase shift and optical density OD as a function of the peak pump laser intensity for 35 fs BWL pulses together with a fit taking a 5-photon ionization process into account (solid lines). On the right scale the calculated free electron density assuming a homogeneous distribution (realistic only for low laser intensities) is also shown. The light gray window represents the intensity in which an electron collision time of (1.6 ± 0.3) fs was determined. In this intensity regime, both the OD and the phase shift follow the power law I^5.

The phase shift reaches a maximum at pump peak intensity of $4.8\cdot10^{12}\,\mathrm{W\,cm^{-2}}$ and starts to decrease for higher values. This behavior was also observed for solid dielectrics [22] [45] and was attributed to a strong inhomogeneous distribution of free electron density in longitudinal direction (in contrast to the assumption of homogenous excitation made above). This can be substantiated by the observation of visible localized plasma

spark inside the water at $9.6 \cdot 10^{12}\,\mathrm{W\,cm}^{-2}$. Also, previous studies reported an averaged threshold intensity of $6.6 \cdot 10^{12}\,\mathrm{W\,cm}^{-2}$ for which the longitudinal distribution of high density free electron plasma is on the order of 1 µm [49] and thus much smaller than the sample thickness of our water jet.

The optical density shows roughly the same dependence on the pump laser intensity as the phase shift. From the two curves the Drude collision time can be extracted; the value was measured to be $\tau_c = (1.6 \pm 0.3)\mathrm{fs}$ [24] for the intensity range indicated in Fig. 7, where the assumption of a homogeneous distribution is reasonable. This value is in good agreement with values presented in the literature, ranging from 1.2 fs [49] to 1.7 fs [50].

Third-order dispersion shaped pulses

Temporally asymmetric laser pulses and their temporal inverted counterparts show quite different effects than band width limited pulses of the same pulse energy. The measured dependence of phase shift on pump pulse energy can be seen in figure 8. The threshold value for TOD shaped pulses is higher than for the BWL pulse due to the decreased peak laser intensity (compare Fig. 3 in section 4.2.2). It can also be seen, that for identical pump pulse energy the absolute phase shift induced by positive TOD shaped pulses is higher than the one corresponding to the negative TOD.

Furthermore the maximum phase shift produced by positive TOD is considerably higher than for negative TOD or BWL pulses. Seeing that the trend of phase shift is in each case continuously falling after the maximum is reached, even the band width limited pulse with its high peak intensity is at no pulse energy as effective as the positive TOD pulse. This is a strong indication that temporally shaped pulses can be used to optimize the transfer of the laser pulse energy into the transparent dielectric, which merits further investigation.

In addition to the above mentioned experiments a basic rate equation model was employed to simulate the laser excitation and the optical properties in the range of homogeneous excitation [24]. By applying the different pulse shapes (namely BWL and $\pm 6 \cdot 10^{5}\,\mathrm{fs}^{3}$ TOD) we were able to extract, for the first time, the multi-photon and avalanche ionization coefficients of water. The simulated and measured curves showed a very good agreement, as seen in Fig. 8B.
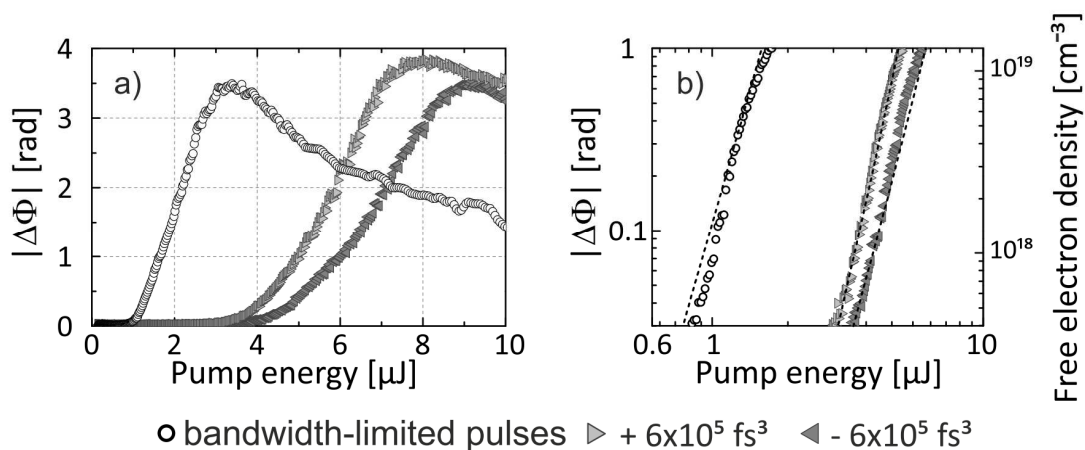
Fig. 8: Dependence of the absolute phase shift on the pulse laser energy for BWL 35 fs pulses and $\pm 6 \cdot 10^{5}\,\mathrm{fs}^{3}$ third order dispersion shaped pulses in linear representation. Positive cubic shaped pulses produce a higher phase shift than negative ones for the same total energy (tilt of triangles indicate sign of dispersion) (a). Excerpt of (a) in double logarithmic representation from region of homogeneous excitation. Black dashed lines show simulation based on a generic rate equation model (b).

It was shown how highly intense laser pulses interact with large band gap dielectric materials and how the selective manipulation of the temporal intensity distribution can control the ionization processes. With this powerful tool, it was demonstrated that the creation of sustainable material modification of fused silica one order below the diffraction limit is possible.

In the following part a useful application of this tool and which advantages it has compared to conventional methods in the creation of photonic structures is presented.

4.2.4 Fabrication of a photonic crystal based filter device by temporally shaped fs-laser pulses

As a demonstration of the potential that material processing by temporally shaped fs-laser pulses bears for optical applications, the fabrication of a typical device structure is investigated. The structure consists of a dielectric thin-film with a 2D photonic crystal pattern, employing the excitation of Fano resonances for a narrow-band spectral filter element.

Fano resonances are observed, when a resonant state is superposed to a continuous state [51] [52]. In an optical implementation, a thin film with higher refractive index than the surrounding medium is acting as a slab waveguide. Waves with normal incident to the layer cannot couple to a waveguide mode due to their orthogonal properties. By structuring the slab waveguide with a periodic pattern the incident wave can couple resonantly to a waveguide mode if the matching conditions are fulfilled [53]. Since the coupling takes place in both directions, the mode is not truly guided by the slab, but is considered as a leaky-mode. Thus the resonant mode is coupling out of the slab again and superposes with free-space modes of directly transmitted or reflected waves. Fano resonances often show asymmetric spectral behavior, stemming from the phase change in the resonance of the coupled leaky-mode. Spectral position, width, strength and shape of the Fano resonance can be tailored by designing the slab waveguide and periodic structure accordingly. In our device we implement a 2D photonic crystal pattern with a square lattice and circular base elements to obtain a polarization independent narrow-band filter. The advantage of such an element is the very compact design, which consists of only one structured dielectric layer on a substrate material. Comparable filter elements are based on a Fabry-Pérot configuration, consisting of several ten layers surrounding a cavity. Additionally, polarization dependency can be introduced to a Fano filter by designing the periodic structure with a broken symmetry. All these properties are beneficial for application in e.g. MEMS devices or on the tip of an optical fiber [54] [55].

Impact of fs-laser pulse processing on the implementation of photonic crystals

The fabrication of a Fano filter structure using the conventional technologies is based mainly on three processing steps. First a single layer or multiple thin-films are deposited which form the slab waveguide. Subsequently, the photonic crystal pattern is generated by lithography and transferred to the slab waveguide by anisotropic dry etching.

If ablation by temporally shaped fs-laser pulses is employed for the fabrication of Fano resonant structures, several constraints have to be considered and investigated. Due to the relation of the ionization processes to the band gap energy a clear material dependency exists. Therefore in the first approach structures are solely created in a single material. For our experiments we chose SiO_2 which has already been studied in our previous investigation on the fs-laser induced ablation process [compare Sec. 4.2.2]. Since we receive by this method a periodic pattern in a low-index material, a high-index layer has to be coated on top to obtain the required slab waveguide. During the deposition of this layer the high-index material is also partly filling the ablated hole structures, leading to a periodic modulation of the waveguide core as well. Another important parameter which affects the performance of the Fano filters is the shape and profile of the laser generated base elements. Characterization of ablated structures generated by TOD fs-laser pulses show a funnel shape in the top section

with a small rim at the surface. The deeper section of the hole forms a narrow and parallel channel that can exhibit rather high aspect ratios (Fig 10a). A final remark must be made on the refractive indices of the available materials. Since SiO_2 is used as substrate and high-index thin-films are restricted to indices below n= 2.3, only a low index contrast of approx. $\Delta n=0.8$ can be exploited. This is a further challenge when designing the Fano filter. Air-bridged elements, which could increase the index contrast, are not implemented due to the commonly observed bending problems based on high mechanical stresses.

For further investigations material processing of a thin-film on top of the substrate material is very promising. This would not only provide a method to fabricate Fano filters and similar devices directly in the target material, but could be used for generation of structured hard masks for further etching steps as well. If the ablation process in thin-films can be controlled to be sufficiently material dependent, selective structuring of one material without damaging other materials becomes possible.

Theoretical model calculations of realistic filter devices

Fundamental investigations on the particular properties of photonic crystal structures generated by fs-laser pulse processing and optimized design parameters for Fano filter devices were obtained by numerical simulations. We utilize the 3D finite-difference time-domain method (FDTD) [56] which provides the distribution and propagation of fields in the time domain and the spectral properties by applying a harmonic inversion. Mainly three base models were implemented to be able to efficiently address the complexity of different investigated problems. 1) The principle characteristics of photonic crystal structures can be calculated by using a unit cell of the periodic pattern and applying periodic boundary conditions. If the device and source can be assumed to be uniform, this model delivers very good results with reasonable numerical efforts. 2) Finite samples and sources with defined profiles can be simulated by using a slice of the real device, with one or only few unit cells thickness, as model domain. For the other spatial directions the structure is defined with the true parameters and only in direction of the slice thickness periodic boundary conditions are implemented. 3) Full information on the behavior of devices with certain 3D shapes and source properties, like exact spot profiles, were investigated by applying a true 3D model of the full structure. This approach clearly delivers the best results, but is restricted by its very high demand on the computing capacities.

First numerical calculations were performed to analyze the possible parameter regime for Fano resonances in material systems with low refractive index contrast. Various parameters were tested, such as refractive index combinations, layer thicknesses, hole depth and diameter as well as lattice geometries. For symmetric slab waveguides with a low index material on top and for asymmetric configurations with a direct core-to-air interface on top, Fano resonances with different strengths and spectral widths can be excited. These results were used as base for our further implementations of Fano filters.

Models concerning a deposited layer on top of a previously structured photonic crystal array were investigated next. The variation of the pre-existing hole structures and the amount of high index layer material reaching into it showed that for this technological approach still Fano resonances with good quality are obtainable.

Finally, the particular shape of the ablated structures with the funnel-like entrance, the narrow channel with high aspect ratio in the lower part and the forming rim at the surface were defined by considering the characterization of the actual results of fs-laser pulse ablation (Fig. 9a). It could be shown that the rim and funnel-like shape in the top section is not affecting the potential to excite Fano resonances or even limits their quality (Fig. 9b). The high aspect ratio of the narrow channel becomes rather beneficial as this section is only filled partly with the high index layer material and stays void below. This results in a reduced effective index of the substrate material and hence increases the index contrast to the waveguide core considerably.
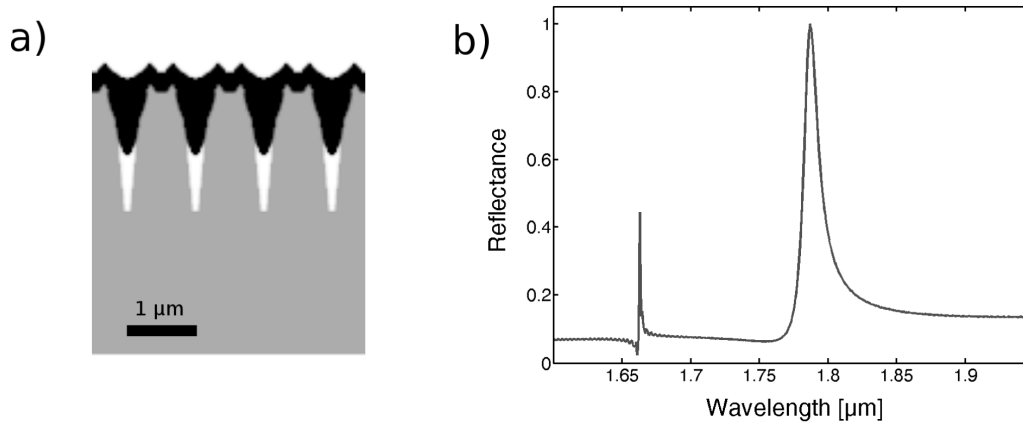
Fig. 9: Simulation model of a photonic crystal structure with realistic structure profile, including the rim formation and funnel shaped top section (a). Numerical result of a filter spectrum which has been obtained from the simulation model (left side) and exhibits a strong Fano resonance at 1.78 µm wavelength (b).

In summary, numerical calculations indicate that photonic crystal structures in low index dielectric materials can be designed to exhibit strong Fano resonances. The fabrication of such devices by temporally shaped fs-laser pulses proves to be feasible, as neither the deposition of the high-index layer on the hole arrays nor the actual hole profiles render a serious problem in the design process. The high aspect ratio of the structures created by TOD pulses even improves the performance of photonic crystal devices due to a lowered effective index of the substrate material.

Investigation on the reduction and avoiding of rim formation

One current drawback of the ablated structures is the formation of a rim around the created hole at the surface. This property may be an obstacle if a very high quality of densely placed array structures is desired, as the rim areas can overlap and influence the optical performance or even the ablation process at neighboring positions (Fig. 10b). Therefore we propose different strategies to either avoid, reduce or remove the rim.

Our first approach is to remove the rim after structuring the sample by either dry or wet chemical etching processes. The notion is to make use of different etch rates in the rim area and the substrate. Although both consist originally of the same material, the ablation process may damage the material in the rim to weaken its etch resistivity. Additionally, elevated or isolated small features often show faster etching due to the surface/volume ratio and tip effects. In the experiments, however, the removal of the rim was always accompanied by severe damage of the generated hole structure, making this method unfeasible.

In the next tests we deposited a thin layer of a material with the same or similar band gap energy on top of the substrate prior to fs-laser pulse processing. If the light matter interaction is not influenced by the additional layer, the rim forms on top of this extra layer. Afterwards, selective etching can be used to remove the top „sacrificial" coating and a clean hole array is obtained. Results of this investigation still exhibited the undesired degradation of the fabricated structures, although the occurrence of etching defects is clearly reduced.

A third investigated method is based on an additional top layer that reduces or avoids the formation of a rim. In previous experiments different substrate materials revealed different behavior regarding the rim. For Al_2O_3 for example the rim is barely noticeable whereas for SiO_2 a strong formation is observable. Therefore experiments with various top-layer materials and thicknesses were carried out, showing that a reduction of the rim formation can be obtained if appropriate combinations of layer material, thickness and pulse energy are applied.

4.2.5 Characterization of ablation channels by focused ion beam milling

The experimental results of fs-laser pulse structuring have been previously characterized by two techniques: SEM and AFM. Both methods are very capable to provide high resolution surface information but struggle to give information about the depth and shape of the generated holes. Even with a high aspect ratio tip, the AFM measurements of sub-100 nm structures are still limited to several ten nanometers of depth.
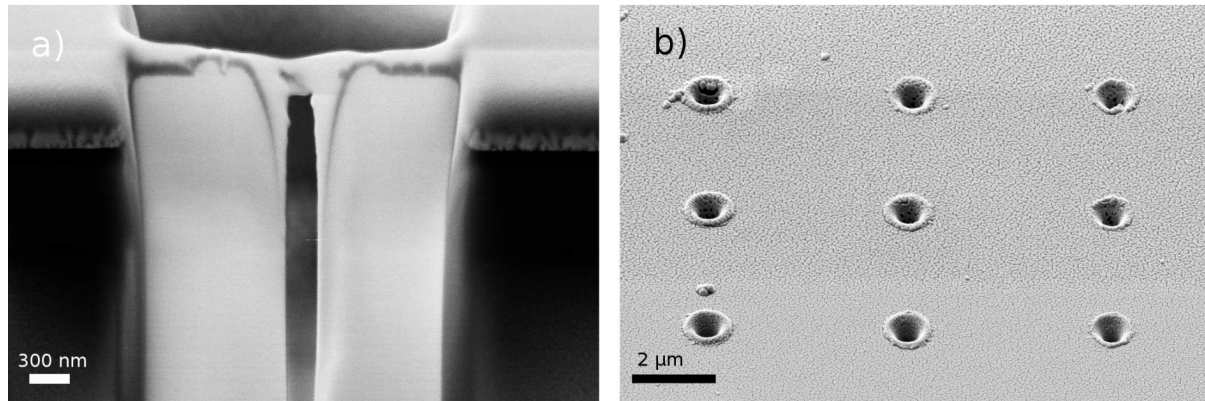
Fig. 10: SEM micrograph of a FIB cross-section showing the top section of an hole structure ablated by temporally shaped (TOD) fs-laser pulses in SiO$_2$ (left). Top view of a photonic crystal array which was fabricated using the presented fs-laser structuring method. The formation of the rim around each hole element at the sample surface can be clearly observed (right).

A very powerful technique to obtain insight to the inner volume of samples is the preparation by Focused Ion Beam milling (FIB) (Fig. 10a). Typically, an ion optical system with liquid Ga$^+$ metal source is attached to an electron optical system. In this two beam configuration alignment and processing of samples can be carried out by direct inspection and images acquired during and after the preparation. The highly accelerated ions are focused on the sample surface and can sputter the material directly with resolutions down to the nanometer range. If the ion current or acceleration voltage is reduced the sputtering process turns from deep milling towards high quality polishing. A gas injection system, which locally emits gas precursors in the focus region offers the option for ion beam induced deposition of materials or gas enhanced ion milling for higher yield and quality [7].

For the preparation of fs-laser pulse generated hole structures the high local resolution and precise alignment, the quality of polished surfaces and possibilities to utilize different detectors of the SEM system are the main advantages. On the other hand, surface charging has again to be addressed, e.g. by coating a thin conductive layer on top of the sample. Also the geometric fidelity of the measured structure parameters has to be verified accurately, since deviations during processing, like a tilt in the final polishing step, may affect the visible projection of the structure. It has to be mentioned of course, that FIB preparation by milling and polishing is a destructive process and cannot be reverted. Depending on the applied technique, the process can also be rather time consuming, limiting the number of samples to inspect. Three different approaches are used in our investigation.

1) Preparation of cross-sections by ion beam milling and subsequent surface polishing. First a protection layer is deposited locally with the gas injection system. A rough gap is milled in the vicinity of the target structure to provide visible access to the depth profile of the hole. Low current polishing is applied until the center of the target structure is reached. This method is comparably fast and offers insight to most geometric parameters, like depth, width and shape.

2) Milling and polishing from both sides results in a thin lamella structure with less than 100 nm thickness. The procedure is analogous to the preparation of cross-sections, but provides a sample with better contrast, as scattering is reduced and back-scattered and secondary electrons can be detected with good selectivity. Additionally, the lamella can be transferred to a copper grid by a lift-out process step and investigated in a TEM or STEM to obtain information on the morphology.

3) Full 3D information of the target structure by FIB tomography. The procedure is similar to the preparation of cross-sections, but after polishing for approx. 10 nm the process is interrupted and a SEM image acquired. Polishing and image acquisition are repeatedly carried out in a loop, starting in front of the target structure and ending after fully removing it. The single images represent each a slice of the structure and a stack of all slices can be compiled by software to reconstruct a 3D model of the ablation channel. However, this preparation technique is destroying the investigated structure completely and is by far the most time consuming approach.

Summary

We demonstrated a sustainable method making use of temporally shaped femtosecond laser pulses to create structures down to the sub-100 nm scale in dielectrics. Our investigations showed that the approach is suitable to create optical elements for the visible wavelength range by direct laser writing. Due to the diffraction limit and charging effects in dielectric materials, it is difficult to reach structures in the sub-100 nm range by conventional production methods.

References

[1]   E. Hecht, Optik, 6., verb. Aufl ed., München: De Gruyter, 2014, pp. XVII, 1125 S..

[2]   S. Kasap and P. Capper, Springer Handbook of Electronic and Photonic Materials, S. Kasap and P. Capper, Eds., Berlin: SPRINGER, 2006, pp. V-1306.

[3]   J. D. Joannopoulos, S. G. Johnson, J. N. Winn and R. D. Meade, Photonic Crystals, vol. 2, Princeton University Press, 2008, pp. i-286.

[4]   K. B. Crozier, V. Lousse, O. Kilic, S. Kim, S. H. Fan and O. Solgaard, "Air-bridged photonic crystal slabs at visible and near-infrared wavelengths," *Phys.Rev.B,* vol. 73, no. 11, p. 115126, 2006.

[5]   G. A. Niklasson, C. G. Granqvist and O. Hunderi, "Effective Medium Models for the Optical-Properties of Inhomogeneous Materials," *Appl.Opt.,* vol. 20, no. 1, pp. 26-30, 1981.

[6]   L. Novotny and B. Hecht, Principles of Nano-Optics, vol. 2nd, Cambridge University Press, 2012.

[7]   L. A. Giannuzzi and F. A. Stevie, Introduction to Focused Ion Beams Instrumentation, Theory, Techniques and Practice, Springer New York, 2005, pp. V-357.

[8]   T. Djenizian and P. Schmuki, "Electron beam lithographic techniques and electrochemical reactions for the micro- and nanostructuring of surfaces under extreme conditions," *J.Electroceram,* vol. 16, no. 1, pp. 9-14, 2006.

[9] R. Wollhofen, J. Katzmann, C. Hrelescu, J. Jacak and T. A. Klar, "120 nm resolution and 55 nm structure size in STED-lithography," *Optics Express,* vol. 21, no. 9, pp. 10831-10840, 2013.

[10] P. van Zant, Microchip fabrication, vol. 6, McGraw-Hill, 2014.

[11] L. Englert, B. Rethfeld, L. Haag, M. Wollenhaupt, C. Sarpe-Tudoran and T. Baumert, "Control of ionization processes in high band gap materials via tailored femtosecond pulses," *Optics Express,* vol. 15, no. 26, p. 17855, 2007.

[12] M. Lenzner, J. Krüger, S. Sartania, Z. Cheng, C. Spielmann, G. Mourou, W. Kautek and F. Krausz, "Femtosecond Optical Breakdown in Dielectrics," *Physical Review Letters,* vol. 80, no. 18, pp. 4076-4079, 1998.

[13] B. C. Stuart, M. D. Feit, A. M. Rubenchik, B. W. Shore and M. D. Perry, "Laser-Induced Damage in Dielectrics with Nanosecond to Subpicosecond Pulses," *Physical Review Letters,* vol. 74, no. 12, pp. 2248-2251, 1995.

[14] A. C. Tien, S. Backus, H. Kapteyn, M. Murnane and G. Mourou, "Short-pulse laser damage in transparent materials as a function of pulse duration," *Physical Review Letters,* vol. 82, no. 19, pp. 3883-3886, 1999.

[15] B. Rethfeld, "Unified model for the free-electron avalanche in laser-irradiated dielectrics," *Physical Review Letters,* vol. 92, no. 18, p. 187401, 2004.

[16] B. Rethfeld, "Free-electron generation in laser-irradiated dielectrics," *Physical Review B,* vol. 73, no. 3, p. 035101, 2006.

[17] M. Wollenhaupt, L. Englert, A. Horn and T. Baumert, "Control of Ionization Processes in High Band Gap Materials," *Journal of Laser Micro / Nanoengineering,* vol. 4, pp. 144-151, 2009.

[18] L. Englert, M. Wollenhaupt, C. Sarpe, D. Otto and T. Baumert, "Morphology of nanoscale structures on fused silica surfaces from interaction with temporally tailored femtosecond pulses," *Journal of Laser Applications,* vol. 24, no. 4, p. 042002, 2012.

[19] A. M. Weiner, "Femtosecond pulse shaping using spatial light modulators," *Rev.Sci.Instr.,* vol. 71, no. 5, pp. 1929-1960, 2000.

[20] M. Wollenhaupt, A. Assion and T. Baumert, "Femtosecond Laser Pulses: Linear Properties, Manipulation, Generation and Measurement," in *Springer Handbook of Lasers and Optics*, Springer New York, 2007, pp. 937-983.

[21] M. Krug, T. Bayer, M. Wollenhaupt, C. Sarpe-Tudoran, T. Baumert, S. S. Ivanov and N. V. Vitanov, "Coherent strong-field control of multiple states by a single chirped femtosecond laser pulse," *New J.Phys.,* vol. 11, p. 105051, 2009.

[22] S. S. Mao, F. Quéré, S. Guizard, X. Mao, R. E. Russo, G. Petite and P. Martin, "Dynamics of femtosecond laser interactions with dielectrics," *Applied Physics A,* vol. 79, no. 7, pp. 1695-1709, 2004.

[23] P. Balling and J. Schou, "Femtosecond-laser ablation dynamics of dielectrics: basics and applications for thin films," *Reports on Progress in Physics,* vol. 76, no. 3, p. 036502, 2013.

[24] C. Sarpe, J. Köhler, T. Winkler, M. Wollenhaupt and T. Baumert, "Real-time observation of transient electron density in water irradiated with tailored femtosecond laser pulses," *New Journal of Physics,* vol. 14, p. 075021, 2012.

[25] M. Wollenhaupt, A. Assion and T. Baumert, "Chap. 12," in *Springer Handbook of Lasers and Optics*, Springer New York, 2012, pp. 1047-1094.

[26] M. Wollenhaupt, L. Englert, A. Horn, T. Baumert, J.-J. Song, K.-T. Tsen, M. Betz and A. Y. Elezzabi, "Temporal femtosecond pulse tailoring for nanoscale laser processing of wide-bandgap materials," *Proc. SPIE,* vol. 7600, pp. 76000X–76000X-11, 2010.

[27] J. Köhler, M. Wollenhaupt, T. Bayer, C. Sarpe and T. Baumert, "Zeptosecond precision pulse shaping," *Optics Express,* vol. 19, no. 12, pp. 11638-11653, 2011.

[28] L. Englert, M. Wollenhaupt, L. Haag, C. Sarpe-Tudoran, B. Rethfeld and T. Baumert, "Material processing of dielectrics with temporally asymmetric shaped femtosecond laser pulses on the nanometer scale," *Applied Physics A,* vol. 92, no. 4, pp. 749-753, 2008.

[29] A. Couairon, L. Sudrie, M. Franco, B. Prade and A. Mysyrowicz, "Filamentation and damage in fused silica induced by tightly focused femtosecond laser pulses," *Phys.Rev.B,* vol. 71, no. 12, pp. 125435-125435-11, 2005.

[30] Y. V. White, X. Li, Z. Sikorski, L. M. Davis and W. Hofmeister, "Single-pulse ultrafast-laser machining of high aspect nano-holes at the surface of SiO_2," *Optics Express,* vol. 16, no. 19, p. 14411, 2008.

[31] B. Delobelle, F. Courvoisier and P. Delobelle, "Morphology study of femtosecond laser nano-structured borosilicate glass using atomic force microscopy and scanning electron microscopy," *Optics and Lasers in Engineering,* vol. 48, pp. 616-625, 2009.

[32] A. Couairon and A. Mysyrowicz, "Femtosecond filamentation in transparent media," *Physics Reports,* vol. 441, no. 2-4, pp. 47-189, 2007.

[33] A. Assion, M. Wollenhaupt, L. Haag, F. Mayorov, C. Sarpe-Tudoran, M. Winter, U. Kutschera and T. Baumert, "Femtosecond laser-induced breakdown spectrometry for Ca2+ analysis of biological samples with high spatial resolution," *Appl.Phys.B,* vol. 77, no. 4, pp. 391-397, 2003.

[34] A. Präkelt, M. Wollenhaupt, A. Assion, C. Horn, C. Sarpe-Tudoran, M. Winter and T. Baumert, "Compact, robust and flexible setup for femtosecond pulse shaping," *Rev.Sci.Instr.,* vol. 74, no. 11, pp. 4950-4953, 2003.

[35] B. J. Sussman, R. Lautsen and A. Stolow, "Focusing of light following a 4-f pulse shaper: Considerations for quantum control," *Phys.Rev.A,* vol. 77, pp. 043416-043416-11, 2008.

[36] T. Bayer, M. Wollenhaupt and T. Baumert, "Strong-field control landscapes of coherent electronic excitation," *J.Phys.B,* vol. 41, pp. 074007-074007-13, 2008.

[37] T. Bayer, M. Wollenhaupt, C. Sarpe-Tudoran and T. Baumert, "Robust Photon Locking," *Physical Review Letters,* vol. 102, pp. 023004-1-023004-4, 2009.

[38] C. A. Sacchi, "Laser-induced electric breakdown in water," *J. Opt. Soc. Am. B,* vol. 8, no. 2, pp. 337-345, 1991.

[39] C. G. Elles, A. E. Jailaubekov, R. A. Crowell and S. E. Bradforth, "Excitation-energy dependence of the mechanism for two-photon ionization of liquid H2O and D2O from 8.3 to 12.4 eV," *J.Chem.Phys.,* vol. 125, pp. 044515-1-044515-12, 2006.

[40] E. Tokunaga, A. Terasaki and T. Kobayashi, "Frequency-domain interferometer for femtosecond time-resolved phase spectroscopy," *Opt.Lett.,* vol. 17, no. 16, pp. 1131-1133, 1992.

[41] P. Martin, S. Guizard, P. Daguzan, G. Petite, P. D'Oliveira, P. Meynadier and M. Perdix, "Subpicosecond study of carrier trapping dynamics in wide-band-gap crystals," *Phys.Rev.B,* vol. 55, no. 9, pp. 5799-5810, 1997.

[42] P. Audebert, P. Daguzan, A. Dos Santos, J. C. Gauthier, J. P. Geindre, S. Guizard, G. Hamoniaux, K. Krastev, P. Martin, G. Petite and A. Antonetti, "Space-Time Observation of an Electron-Gas in SiO2," *Physical Review Letters,* vol. 73, no. 14, pp. 1990-1993, 1994.

[43] F. Quéré, S. Guizard and P. Martin, "Time-resolved study of laser-induced breakdown in dielectrics," *Europhys.Lett.,* vol. 56, no. 1, pp. 138-144, 2001.

[44] V. V. Temnov, K. Sokolowski-Tinten, P. Zhou and D. Linde, "Femtosecond time-resolved interferometric microscopy," *Appl.Phys.A,* vol. 78, no. 4, pp. 483-489, 2004.

[45] V. V. Temnov, K. Sokolowski-Tinten, P. Zhou, A. El-Khamhawy and D. Linde, "Multiphoton Ionization in Dielectrics: Comparison of Circular and Linear Polarization," *Physical Review Letters,* vol. 97, p. 237403, 2006.

[46] J. Siegel and J. Solis, "Chap. 2," in *Femtosecond Laser Micromachining*, Springer-Verlag Berlin Heidelberg, 2012, pp. 19-41.

[47] M. A. van Dijk, M. Lippitz, D. Stolwijk and M. Orrit, "A common-path interferometer for time-resolved and shot-noise-limited detection of single nanoparticles," *Optics Express,* vol. 15, no. 5, pp. 2273-2287, 2007.

[48] M. Born and E. Wolf, Principles of optics -electromagnetic theory of propagation, interference and diffraction of light, vol. 7th (exp.), Cambridge University Press, 1999, pp. 1-952.

[49] C. Sarpe-Tudoran, A. Assion, M. Wollenhaupt, M. Winter and T. Baumert, "Plasma dynamics of water breakdown at a water surface induced by femtosecond laser pulses," *Applied Physics Letters,* vol. 88, no. 26, p. 261109, 2006.

[50] A. Vogel, J. Noack, G. Huttman and G. Paltauf, "Mechanisms of femtosecond laser nanosurgery of cells and tissues," *Applied Physics B: Lasers and Optics,* vol. 81, no. 8, pp. 1015-1047, 2005.

[51] U. Fano, "Effects of Configuration Interaction on Intensities and Phase Shifts," *Physical Review,* vol. 124, no. 6, pp. 1866-1878, 1961.

[52] A. E. Miroshnichenko, S. Flach and Y. S. Kivshar, "Fano resonances in nanoscale structures," *Reviews of Modern Physics,* vol. 82, no. 3, pp. 2257-2298, 2010.

[53] A. Hessel and A. A. Oliner, "A New Theory of Wood's Anomalies on Optical Gratings," *Applied Optics,* vol. 4, no. 10, p. 1275, 1965.

[54] A. Gellineau, Y.-P. Wong, A. Wang, M. J. Butte and O. Solgaard, "Miniature Fiber Facet Atomic Force Mircoscope Using Photonic Crystal Sensors," *International Conference on Optical MEMS and Nanophotonics,* pp. 3 -4, 2014.

[55] T. Kusserow, Yousuf Khan, R. Zamora, F. Messow and H. Hillmer, "Guided-mode resonances in dielectric photonic crystal slabs with low index contrast," 2012, pp. 170-171.

[56] A. F. Oskooi, D. Roundy, M. Ibanescu, P. Bermel, J. D. Joannopoulos and S. G. Johnson, "Meep: A flexible free-software package for electromagnetic simulations by the FDTD method," *Computer Physics Communications,* vol. 181, no. 3, pp. 687-702, 2010.

[57] D. Otto, "Sub-100 Nanometer-Strukturen via Femtosekunden-Doppelpulse," Master Thesis, Universität Kassel, 2014.